JOURNAL OF GUIDANCE, CONTROL, AND DYNAMICS
Vol. 25, No. 2, March–April 2002

Output Feedback Control of the Nonlinear Aeroelastic Response of a Slender Wing

Mayuresh J. Patil* and Dewey H. Hodges†
Georgia Institute of Technology, Atlanta, Georgia 30332-0150

The design of optimal constant gain output feedback-based controllers for a nonlinear aeroelastic system is presented. Controllers are designed for flutter suppression as well as gust-load alleviation. This controller architecture is one of the simplest, using direct feedback of the sensor outputs, but its performance is highly dependent on sensor selection and placement. Also, the optimal design of such controllers requires an accurate knowledge of the expected disturbance mode and gust spectrum. Results pertaining to the performance of these controllers for aeroelastic control (linear and nonlinear) are presented and compared to those of optimal linear quadratic regulator (LQR) and linear quadratic Gaussian (LQG) controllers. Controllers are designed for various sensor placements. The gain and phase margins of the various controllers are also presented to understand the robustness characteristics. For optimal sensor placement, and with knowledge of the disturbance, the constant gain output feedback controller performance and robustness was found to be equivalent to that of LQR and LQG controllers for the example considered. These controllers were also shown to be very easy to alter and combine with other controllers/filters for better overall system response.

Introduction

ACTIVE aeroelastic control has been a topic of active research for the past two decades. Control design for flutter suppression and gust-load alleviation has been a focus of many researchers, for example, Mukhopadhyay[1] and Lin et al.[2] Most of the control synthesis in previous investigations has been accomplished by linear optimal control theory, specifically linear quadratic regulator (LQR) and linear quadratic Gaussian (LQG) control architecture. An LQR design is not practical because it requires knowledge of the complete state space. In most of the practical aeroelastic control problems it is impossible to sense all of the states of the system. On the other hand, LQG controllers are dynamic controllers that have the same order as the assumed plant. Real-time implementation of high-order controllers is also quite problematic.

There has not been much work focusing on the use of optimal static (constant gain) output feedback (SOF) controllers in aeroelastic applications. Waszak and Srinathkumar[3] and Mukhopadhyay[4] have designed a classical controller based on constant gain output feedback coupled with pole-zero placement to achieve flutter suppression. In the present work, SOF controllers are based on linear quadratic optimization theory and lead to optimal performance with low controller complexity. SOF controllers feed back a linear combination of the sensor outputs and, thus, are very easy to implement. The use of SOF in aeroelastic flutter suppression and gust alleviation systems would lead to considerable simplification of the control law and ease in implementation.

Because of the simplicity of SOF controllers, they can be easily changed as well as combined with other control systems to get better overall characteristics. For example, excellent controller gain rolloff at high frequencies can be achieved by combining an SOF controller with a low-pass filter. SOF controllers can also be used with gain scheduling to generate efficient nonlinear control. On the other hand, SOF controllers use direct feedback of the sensor outputs, and, thus, sensor placement plays a very important role in such controllers. To achieve maximum performance the sensors need to be placed in the best possible location to sense the most important variables. Also, unlike an LQR controller, SOF controllers are optimal only for the assumed disturbance (to the system) and, thus, are not robust to disturbance uncertainty.

This paper presents results pertaining to the performance of SOF controllers in aeroelastic control (linear and nonlinear) and compares their performance to that of LQR and LQG controllers. The SOF controllers are designed for various sensor placements. The gain and phase margins of SOF controllers are also presented to understand the robustness characteristics.

Nonlinear Aeroelastic Model

The aeroelastic model developed in Ref. 5 is used in the present work. The aeroelastic model is used to generate a nominal model based on the linearized aeroelastic system equations. This model is used for control synthesis. In its complete nonlinear form, the model is used to simulate the open-loop as well as closed-loop nonlinear aeroelastic response of the wing.

The structural formulation used in the present research is based on the mixed variational formulation for dynamics of moving beams.[6] Equations of motion are generated by including the appropriate energies in the variational statement followed by application of calculus of variations. The finite state aerodynamic theory of Peters and Johnson[7] is a natural choice for low-order, high-fidelity state-space representation of the aerodynamics. It accounts for large airfoil motion as well as small deformation of the airfoil, for example, trailing-edge flap deflection. The complete aeroelastic formulation is described in detail by Patil[8] and is presented here briefly for the sake of completeness.

The structural equations of motion of the wing can be expressed in terms of a nonlinear structural operator F_S and a nonlinear aerodynamic operator F_L as

$$F_S(\boldsymbol{X}, \dot{\boldsymbol{X}}) - F_L(\boldsymbol{X}, \boldsymbol{Y}, \dot{\boldsymbol{X}}) = 0 \tag{1}$$

where the vector $\boldsymbol{X}$ denotes the set of structural variables and the vector $\boldsymbol{Y}$ denotes the set of aerodynamic induced flow variables. Similarly, we can separate the aerodynamic induced flow equations that model the unsteady wake effects in terms of an induced flow operator F_I and a downwash operator F_W as

$$-F_W(\dot{\boldsymbol{X}}) + F_I(\boldsymbol{Y}, \dot{\boldsymbol{Y}}) = 0 \tag{2}$$

Received 10 March 2000; revision received 16 July 2001; accepted for publication 7 August 2001.

*Postdoctoral Fellow, School of Aerospace Engineering; currently Assistant Professor, Widener University, Chester, PA 19013. Member AIAA.
†Professor, School of Aerospace Engineering. Fellow AIAA.

Specialized Solutions

Equations (1) and (2) represent a set of coupled nonlinear differential equations modeling the dynamics of the coupled aeroelastic system. The solutions of interest can be expressed in the form

$$\begin{Bmatrix} X \\ Y \end{Bmatrix} = \begin{Bmatrix} \bar{X} \\ \bar{Y} \end{Bmatrix} + \begin{Bmatrix} \hat{X}(t) \\ \hat{Y}(t) \end{Bmatrix} \tag{3}$$

where the overbar represents a nonlinear steady-state (equilibrium) solution and the carat represents a linearized perturbation about the nonlinear equilibrium. Such a decomposition of the solution leads to two possibilities: nonlinear (large deformation) static equilibrium and linearized (small perturbation) dynamics at the equilibrium.

Nonlinear Equilibrium Solution

For the steady-state (equilibrium) solution one gets $\bar{\boldsymbol{Y}}$ identically equal to zero [from Eq. (2)]. Thus, one has to solve a set of algebraic nonlinear equations given by

$$F_S(\bar{\boldsymbol{X}}, 0) - F_L(\bar{\boldsymbol{X}}, 0, 0) = 0 \tag{4}$$

The Jacobian matrix of the preceding set of nonlinear equations can be obtained analytically and is found to be very sparse.[9] The steady-state solution can, thus, be found very efficiently using a Newton–Raphson method.

Linear Small Perturbation Solution

When Eqs. (1) and (2) are perturbed about the calculated nonlinear steady state [using Eq. (3)], the linearized set of equations can be written as

$$\left[\begin{matrix} \dfrac{\partial F_S}{\partial \dot{X}} - \dfrac{\partial F_L}{\partial \dot{X}} & 0 \\ -\dfrac{\partial F_W}{\partial \dot{X}} & \dfrac{\partial F_I}{\partial \dot{Y}} \end{matrix}\right]_{\substack{X=\bar{X} \\ Y=0}} \begin{Bmatrix} \dot{\hat{X}} \\ \dot{\hat{Y}} \end{Bmatrix} + \left[\begin{matrix} \dfrac{\partial F_S}{\partial X} - \dfrac{\partial F_L}{\partial X} & -\dfrac{\partial F_L}{\partial Y} \\ 0 & \dfrac{\partial F_I}{\partial Y} \end{matrix}\right]_{\substack{X=\bar{X} \\ Y=0}} \begin{Bmatrix} \hat{X} \\ \hat{Y} \end{Bmatrix} = \begin{Bmatrix} 0 \\ 0 \end{Bmatrix} \tag{5}$$

These equations describe the small amplitude (linear) dynamics of the system around the calculated (nonlinear) steady state. Now, if the dynamic modes are assumed to be of the form e^{st}, the preceding equations can be solved as an eigenvalue problem to get the damping, frequency, and mode shape of the various modes. The stability condition of the aeroelastic system at various operating trim conditions can, thus, be obtained by perturbing the nonlinear equations of motion about the various nonlinear equilibrium solutions. The preceding set of linear dynamic equations is used as a nominal system to design a linear optimal controller.

Nonlinear Dynamic Solution

To investigate the nonlinear dynamics of the aeroelastic system, a time history has to be obtained using the complete nonlinear equations of motion. Space–time finite elements are used in the present work for time marching.[8] Using space–time finite elements on the complete nonlinear system equations (1) and (2), one gets the time-marching algorithm as a set of nonlinear algebraic equations

$$\begin{aligned} F_S^t(X_i, X_f) - F_L^t(X_i, X_f, Y_i, Y_f) &= 0 \\ -F_W^t(X_i, X_f) + F_I^t(Y_i, Y_f) &= 0 \end{aligned} \tag{6}$$

where subscripts i and f represent the variable values at the initial and final time and F_S^t, F_L^t, F_W^t, and F_I^t are the nonlinear structural, aerodynamics, wake, and inflow operators calculated using space–time finite elements.[10] If the initial conditions and time interval are specified, the variable values at the final condition are obtained by solving the set of nonlinear algebraic equations. These nonlinear time-marching equations are used for open- and closed-loop simulation of the system.

System Order Reduction

Before a controller is designed for the aeroelastic system, the linearized equations of motion (5) of the system need to be converted to a low-order, state-space form. The original total number of variables of the complete nonlinear system (and the linearized form) is around $30 \times n$, where n is the number of finite elements used to model the wing. The break up of the 30 variables for each element is 3 each for displacement u, rotation θ, internal force F, internal moment M, linear momentum P, and angular momentum H and 6 each for induced flow states λ and stall states. For an eight-element model of the wing this total is 240, which is quite large. Some of the equations, for example, the strain–displacement relations, have no time derivatives, and, thus, these equations can be used to represent the force and moment in terms of the displacements and rotations, reducing the order of the system to $24 \times n$. Also, in the nominal conditions considered here, there are no stall states leading to $18 \times n$ variables. The final reduction in the number of variables and equations (and, thus, the order of the nominal system) comes from the fact that the extensional and shear rigidities are very high and, thus, the corresponding strains are negligibly low. Thus, a zero shear and zero extension approximation could be used to write the displacements and linear momentum variables in terms of the rotations and angular momentum variables. This further reduces the number of structural equations in half. The final count of variables is $12 \times n$, which includes three rotational variables and their time derivatives and six induced flow states per element. The displacement variables can always be recovered from the rotation variables.

SOF Controller

SOF controllers are based on direct feedback of the sensor output. Unlike an LQR controller, an SOF design does not assume the availability of all of the system states for feedback. Rather, it is assumed that only a few linear combinations of system states are available (directly from the sensors). An optimal SOF controller aims to find the feedback gains that optimize a given performance index.

A theory supporting the problem of optimal SOF for linear, multivariable systems was first presented by Levine and Athans.[11] A solution technique for solving the nonlinear matrix equations was also presented. A recent paper by Syrmos et al.[12] gives a survey of the various SOF techniques, including optimal SOF. The theory pertaining to optimal SOF is presented here briefly.

Given an nth-order linear time invariant stabilizable system

$$\dot{x}(t) = Ax(t) + Bu(t) + Dw(t), \qquad y(t) = Cx(t) \tag{7}$$

where $x \in \Re^n$ are the system states, A is the system dynamics matrix in state-space form, $u \in \Re^m$ are the actuator commands, B is the control actuation matrix, $y \in \Re^p$ are the sensor measurements, C is the matrix relating the sensor measurements to the state variables, w is zero mean unit intensity white noise process, and D is the matrix of noise intensity.

Assuming constant gain output feedback of the form

$$u(t) = Ky(t) \tag{8}$$

one can determine feedback gains K such that they stabilizes the closed-loop system and minimize the quadratic performance measure given by

$$J(K) = \lim_{t \to \infty} \mathcal{E}\left\{ \frac{1}{t} \int_0^t \left[x^T(\tau) Q x(\tau) + u^T(\tau) R u(\tau) \right] \mathrm{d}\tau \right\} \tag{9}$$

where $Q \geq 0$ and $R > 0$ are state and control weighting matrices.

The solution to the optimization problem just given is

$$K = -R^{-1} B^T S P C^T (C P C)^{-1} \tag{10}$$

where P and S are given by a set of coupled nonlinear matrix equations in terms of system parameters and K. Thus, the calculation of

K involves the solution of three equations including the preceding equation for K and the Lyapunov equations given here

$$0 = A_c^T S + S A_c + Q - C^T K^T R K C$$

$$0 = A_c P + P A_c^T + V \tag{11}$$

where $A_c = A + BKC$ and $V = DD^T$.

The solution of the preceding set of coupled nonlinear equations can be calculated using a variety of iterative algorithms. Only a few of these algorithms have been proved to be convergent to a local minimum. Many other algorithms, though not proven to be convergent, do converge in most of the practical cases. The computational effort required also varies. A detailed survey of the various computational methods used to solve the optimal SOF problem is presented by Makila and Toivonen.[13] Two algorithms have been used in results presented here: the Broyden, Fletcher, Goldfarb, and Shanno algorithm (see Ref. 14) and an algorithm proposed by Moerder and Calise.[15]

Results

The example considered for the results presented in the present work is a high-aspect-ratiowing similar to those likely to be used in high-altitude, long-endurance (HALE) aircraft. HALE aircraft are becoming increasingly common in various civil as well as military roles, including reconnaissance, remote sensing, acting as data relay stations, and so on. However, with the increase in the span of the wing (required for higher lift-to-drag ratio) the wing is likely to encounter various detrimental aeroelastic response and stability problems. The aim of the present example is to present a simple study to illustrate the effective use of SOF for improving the aeroelastic characteristics of slender wings.

HALE Wing Model

The example HALE wing considered is a slender wing of half-span aspect ratio of 16 (chord of 1 m). Figure 1 shows the HALE aircraft under consideration. The stiffness and inertial characteristics of the wing are detailed in Table 1. The nominal flight condition is a speed of 25 m/s at an altitude of 20 km. The flutter speed of the undeformed wing has been determined to be 32.21 m/s at the same altitude (see Ref. 16). The control design goals include 1) extending the flutter envelop (closed-loop flutter speed) to at least 35 m/s by active control and 2) gust-load alleviation at the nominal speed of 25 m/s.

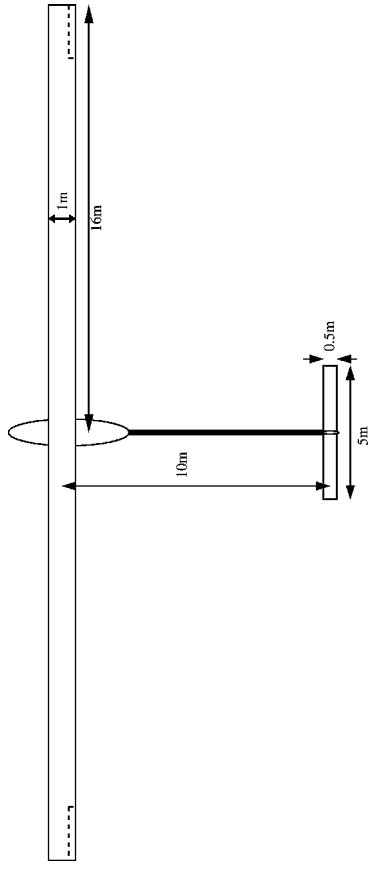

Fig. 1 Aircraft under consideration.

Table 1 Model data

Parameter	Value
Wing	
Half span	16 m
Chord	1 m
Mass per unit length	0.75 kg/m
Mom. inertia (50% chord)	0.1 kg m
Spanwise elastic axis	50% chord
Center of gravity	50% chord
Bending rigidity	2×10^4 N/m^2
Torsional rigidity	1×10^4 N/m^2
Bending rigidity (edgewise)	5×10^6 N/m^2
Flight condition	
Altitude	20 km
Density of air	0.0889 kg/m^3

Sensor and Actuator

Various sensor placement strategies are considered. The aeroelastic system is dominated by the torsion and bending deformations. Thus, twist sensors (for torsion) and curvature sensors (for bending) and the corresponding twist-rate and curvature-rate sensors are used. The SOF controllers are denoted by the sensors used: 1α denotes root-twist and root-twist-rate sensors; 2α denotes twist and twist-rate sensors at the root as well as at the midspan; and 3α denotes twist and twist-rate sensors at the root, one-third spanwise position, and two-third spanwise position. Such an addition of sensors leads to progressively more information on higher modes. The curvature sensors are denoted similarly, with $1h$ denoting the curvature and curvature-rate sensors at the root. Control is achieved by a flap at the wing tip. One of the aims of this paper is to show the effect of sensor placement on the effectiveness of SOF control.

Flutter Suppression

The first study involves flutter suppression for the HALE wing at 35 m/s. The system matrices A, B, and C are obtained by transforming the Jacobian matrix as described in the earlier sections. The controller is optimized for minimum control. Thus, the state is not penalized ($Q = 0$), and the control weight matrix is assumed unity ($R = 1$). A unit amplitude uncorrelated process noise is assumed to affect all of the structural equations of motion equally. Results obtained from an SOF controller are compared to those from an LQR controller. As discussed earlier, an LQR controller cannot be practically implemented because some the states of the system are unknown. Thus, an LQR controller must be accompanied by a state estimator, such as a Kalman filter. Once an estimator is added the resulting dynamic controller increases the controller complexity considerably. Though impractical, an LQR controller gives the best achievable performance and is, thus, a good baseline to gauge the optimality of an SOF controller.

Linear SOF Controller

Table 2 shows the results for control cost and closed-loop damping due to various SOF controllers. As seen in Table 2, the SOF controller using just two-sensor feedback can give very good performance. For example, if one uses just root-twist and root-twist-rate feedback, the system is stabilized with only 7% more cost as compared to an LQR controller, which in turn means only a 3.5% increase in control rms value. Also, the closed-loop damping of the flutter mode is quite close to that provided by an LQR controller. Thus, with the data from just two sensors, the SOF controller is able to control flutter with a control cost close to that of an LQR controller, which for the present example requires 96 states for feedback. As the number of twist sensors is increased, the performance and the stability improves slightly. On the other hand, feeding back

Table 2 SOF performance for various sensor configurations

Sensors configuration	Control cost	% increment in control rms with respect to LQR	Closed-loop eigen value real part	Closed-loop eigen value imaginary part
System	0	——	1.0323	21.1978
LQR	586.90	0%	−1.0323	21.1978
SOF 1α	628.56	3.49%	−0.9190	21.2219
SOF 2α	626.29	3.30%	−0.9118	21.2646
SOF 3α	625.13	3.21%	−0.9167	21.2528
SOF 1h	Unstable	——	——	——
SOF 1α1h	622.33	2.97%	−0.9598	21.2242

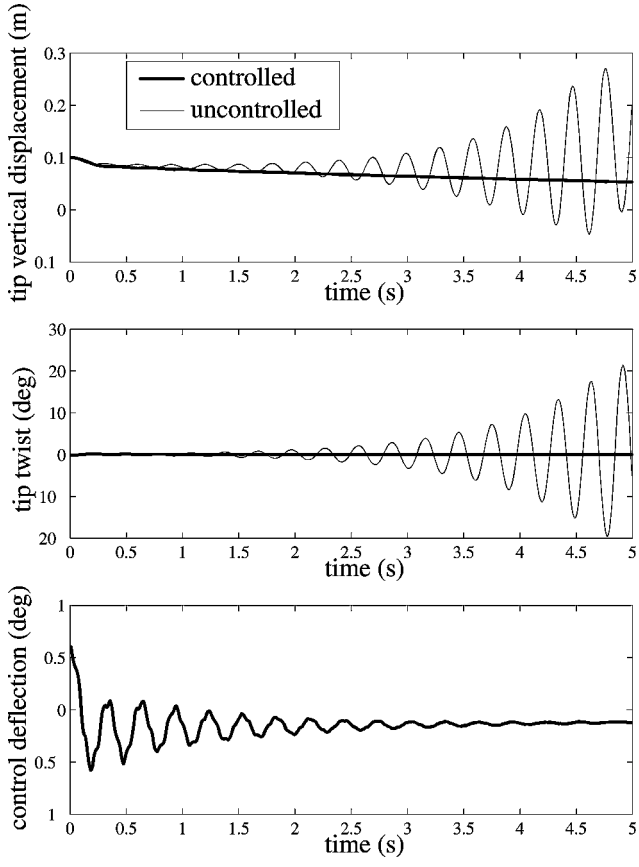

Fig. 2 SOF applied for flutter suppression at flight speed of 35 m/s.

only root-curvature and root-curvature-rate sensors cannot stabilize the system. This is because the aeroelastic energy transfer is dominated by the torsional instability that in turn transfers some energy to the bending mode. Thus, the knowledge of torsional variables is very important for a stabilizing controller design.

To test the controller effectiveness, the HALE wing model is simulated with and without the controller. Figure 2 shows the controlled and uncontrolled time history of the wing at 35 m/s with an initial bending deflection of 0.1 m at the tip. The controller with root-twist and root-twist-rate feedback is used in the simulation presented. The flutter is effectively suppressed by SOF control.

SOF gives a good stabilizing controller with a proper choice of sensors. The performance comparisons with an LQR controller are also quite favorable. However, note that SOF gives the optimal performance for the given disturbance (the same level of disturbance was assumed to be affecting all structural equations), whereas an LQR controller gives the best performance for any disturbance (because the LQR solution is independent of D, the matrix of noise intensity). Thus, if the disturbance were such that the aerodynamic equations were more affected, or that the structural equations were affected in a different mode, then one would not get good performance for the new disturbance using the original SOF controller. However, the performance of the LQR controller is still the best achievable, and, consequently, for a random disturbance the performance of an SOF controller would not be as close to that of an LQR controller. To design an optimal SOF controller, the aeroelastician would have to be able to predict accurately the amount of atmospheric disturbance, which would affect the aeroelastic system.

Nonlinear SOF Controller

Because of the simplicity of the SOF controller, it can be easily combined with gain scheduling to obtain a nonlinear controller. To demonstrate the ease of designing a nonlinear controller with SOF, a simple nonlinear controller is designed to control the nonlinear phenomena of limit-cycle oscillations (LCO). Note here that it is the insight into the nonlinear physical mechanisms responsible for the LCO that leads to a design of a simple nonlinear controller.

Before the design of the nonlinear controller is explained, it is helpful to discuss the nonlinear LCO results presented by Patil et al.[10] They have shown that a wing curved due to lift forces exhibits behavior that is completely different from that of an undeformed wing. In fact, curved wings lead to instability at speeds much lower then the linear flutter speed. The dominant nonlinearity stems from wing bending, as is exhibited in wing tip displacement. The wing model when linearized about trim conditions at various levels of wing tip displacement leads to various linearized systems. The linearized system eigenvalues exhibit drastic changes in the stability of the wing vs bending. For example, the HALE wing at 30 m/s is stable if linear analysis is used. There is a decrease in stability margin with the curving of a beam, and, at a tip displacement of around 0.6 m, it becomes unstable. The tip displacement is, thus, a good parameter on which to base a nonlinear controller. Details on the type of nonlinearity in the wing are given in Ref. 10.

A nonlinear controller is designed using dynamic gain scheduling, based on the tip displacement. A series of SOF controllers are designed at intervals of tip displacement. Again, root strain and root strain rate are fed back, and the controller is linearly interpolated at in-between tip displacements. Figure 3 shows the effect of such a nonlinear controller on the aeroelastic behavior of the HALE wing at 30 m/s when it is disturbed by a tip displacement of 2 m. The uncontrolled case gets attracted to an LCO, but the controlled wing approaches the undeformed stable equilibrium. If the damping of various modes is evaluated, one finds that even without control the first bending mode is damped, so that the bending deformation settles to an equilibrium value. As the wing oscillates about this bent configuration, a torsional mode is excited, causing the wing to gain energy from the flow and transfer it back to the bending modes. The nonlinear SOF controller does not let the torsional energy increase, thus effectively suppressing the torsional mode and avoiding LCOs.

The use of the SOF controller truly simplifies the gain-scheduling mechanism because only two control parameters (i. e., the feedback gains corresponding to root twist and root-twist rate) define the controller. Thus, to implement practically such a gain-scheduled controller, the control computer would have to store a very small number of parameters. If one compares this SOF controller with gain-scheduled, observer-based controllers, the simplicity of SOF controllers is obvious.

Combining SOF with a Low-Pass Filter

Before this section on flutter suppression is ended, the SOF controller is compared to an LQG controller, that is, an LQR controller in series with a Kalman estimator. An LQG controller is an optimal dynamic output feedback controller that gives optimal performance

Table 3 SOF/LPF performance

Sensors configuration	Control cost	% increment in control rms		Closed-loop eigen value real part	Closed-loop eigen value, imaginary part
		with respect to LQR	with respect to LQG		
System	0	——	——	1.0323	21.1978
LQR	586.90	0%	——	−1.0323	21.1978
LQG 1α	607.46	1.74%	0%	−1.0323	21.1978
SOF 1α	626.29	3.49%	1.72%	−0.9190	21.2219
SOF 1α + LPF	796.13	16.47%	14.48%	−0.6438	22.0321
Reoptimized	623.72	3.09%	1.33%	−0.9396	21.2038

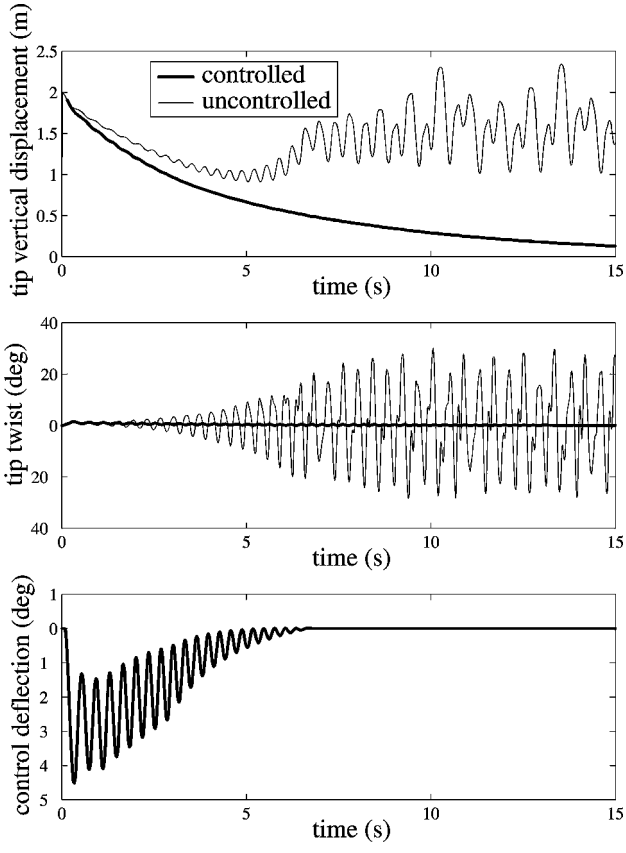

Fig. 3 Nonlinear SOF controller applied to LCO control at 30 m/s.

for the case in which only a few states of the system are sensed. On the other hand, the controller is very complex as compared to simple constant output feedback. Because the SOF controllers are designed under the assumption of zero sensor noise, the LQG controllers are also designed using negligibly small sensor noise (the sensor noise matrix is reduced until the cost converges to a value).

Table 3 shows the performance predictions for an LQG controller compared to SOF controllers. As seen in Table 3, the LQG controller performance is not as good as that of an LQR controller, but is only slightly better than that of an SOF controller. Thus, it is seen that an LQG cannot be preferred over SOF for the small increase in performance because an LQG controller is accompanied by a drastic increase in complexity.

There are some characteristics of LQG controllers that make them a better choice compared to SOF controllers. One of these is the high-frequency rolloff, meaning that the high-frequency unmodeled dynamics of the system are not affected by the controller (controller spillover). Thus, the risk of destabilizing the system at high frequencies is reduced. One can introduce high-frequency rolloff in SOF by using a low-pass filter (LPF) in series with the SOF controller. Such characteristics have been shown earlier for second-order acceleration feedback controllers.[17]

In this example, a fixed, second-order, LPF of frequency cutoff 100 rad/s and damping factor 1.0 is used. As can be expected, such an LPF will change the phase characteristics of the combined controller, thus, leading to a decrease in the controller performance. However, the SOF controller could be reoptimized by assuming it to be attached to an LPF. The reoptimized combination of the LPF and SOF leads to a simple yet very effective controller. As seen in Table 3, the control rms is only 1.33% higher for the LPF plus SOF combination compared to that of an LQG controller, with better rolloff characteristics and a simple implementation.

Table 4 Comparison of the stability margins

Sensors configuration	Gain margins, dB		Phase margins, deg	
LQR	−6.02	+∞	−60	+60
LQG 1α	−5.84	+12.03	−58.70	+56.15
SOF 1α	−5.44	+9.66	−58.98	+54.87
SOF 1α + LPF	−4.30	+9.50	−80.29	+28.36
SOF 1α + LPF (reopt.)	−5.69	+9.81	−59.28	+56.29

Gain and Phase Margins

Finally, one of the most desired properties of a controller is robustness. Robustness leads to reliable controller performance in the face of plant or controller uncertainty. Stability margins are a good indication of the controller robustness to gain and phase shifts. Table 4 shows the stability margin predictions for the various controllers under investigation. As expected, the low-authority LQR controller has a gain margin of −6.02 dB and +∞ dB and a phase margin of ±60 deg. The LQG controller has similar lower gain margins and phase margins. There is a degradation in the upper gain margin to around +12 dB (but still ensuring stability at controller gains up to four times the nominal). As for the SOF controller, it shows gain and phase margins similar to those of the LQG design. Thus, the SOF controller can be expected to have equivalent robustness properties. Adding an LPF to the SOF controller creates a shift in the phase margin. The phase shift is introduced because the LPF itself has a phase shift of around 25 deg at the unstable frequency. This phase shift is overcome by reoptimizing the SOF controller. Such a reoptimized controller regains the characteristics of the stand-alone SOF. Thus, a reoptimized SOF + LPF controller has performance, high-frequency rolloff, and stability margins very close to those of an LQG controller, but without the associated complexity.

To summarize, with the proper choice of sensors, an SOF controller can be designed that has performance close to that of an LQR controller. It is possible to modify the simple SOF controller for control of nonlinear system response. High-frequency rolloff can be achieved by combining such a controller with an LPF. Finally, the SOF controllers also have gain and phase margins equivalent to LQR/LQG controllers. The SOF controllers can, thus, be quite effective for flutter suppression.

Gust-Load Alleviation

An aircraft is exposed to various wind and gust levels, depending on its flight. Such external disturbances lead to a structural response of varying magnitude. The gust-load alleviation problem aims to keep the disturbance response of the wing low. Low disturbance response helps in extending the fatigue life of the structure as well as in improving ride quality.

Gust Model

For the results presented here, the gust model is based on the continuous atmospheric turbulence model given by Bisplinghoff

Table 5 SOF performance for gust alleviation at 25 m/s

Sensors configuration	Performance measure	State cost	Control cost
SOF 1α	74.614	74.215	0.399
SOF 1h	62.788	53.342	9.446
SOF 2h	62.598	53.016	9.582
SOF 3h	62.580	52.985	9.595
SOF 1α1h	62.605	53.033	9.572

et al.[18] With this model, the power spectrum of atmospheric turbulence in terms of space frequency can be represented as

$$\Phi\left(\frac{\omega}{U}\right)\left[\frac{(\text{ft/s})^2}{\text{rad/ft}}\right] = \frac{0.060}{0.000004 + (\omega/U)^2} \tag{12}$$

For a given speed $\bar{U}$, one could write the power frequency spectrum of atmospheric turbulence in SI units as

$$\Phi(\omega)\left[\frac{(\text{m/s})^2}{\text{rad/s}}\right] = \frac{0.078\bar{U}}{0.000043\bar{U}^2 + \omega^2} \tag{13}$$

The preceding equation at a given flight speed has the form of the power spectrum of a first-order dynamic system excited by white noise. Thus, the atmospheric turbulence model can be easily represented in terms of a single-state dynamic system. This equation is added to the aeroelastic system equations. The output of the gust equation to white noise is the source of disturbance to the aeroelastic system.

SOF Design for Gust Alleviation

The HALE wing is considered at nominal flight speed of 25 m/s. The state cost component of the performance index is defined in terms of the structural energy[19] as $J_s = x_s^T[K]x_s + \dot{x}_s^T[M]\dot{x}_s$, where x_s are the structural states.

Table 5 shows the state and control cost associated with SOF controllers using various sensors. The results are very different from those obtained for flutter suppression. For flutter suppression, twist sensing was most important because the unstable mode was dominant in twist. For gust alleviation, curvature (bending) sensing leads to the best performance. Here, the low-frequency bending modes are excited the most by the gust. Curvature sensing is, thus, most important for gust-load alleviation because it senses the modes that are most disturbed.

Comparison with LQR Designs

The way to represent an LQR controller for a system with a gust state is unclear because, even though the gust state is part of the mathematical system that is used for design, it is not a part of the actual system. Thus, whether or not to include the gust state feedback is unclear. There are three LQR-like controllers designs possible. The first one is denoted as LQR (white noise) and is based on the assumption of a white noise disturbance to the system, that is, the gust state equation is not included in LQR design. The second, LQR (gust model), is the LQR design based on the model that includes the gust state. Thus, the controller uses the gust state feedback for control. The third controller, denoted by LQR full state feedback (FSF) assumes the existence of gust state for control design, but the feedback is dependent only on the original aeroelastic system states. All controllers are implemented on the complete aeroelastic system, including the gust model.

Table 6 gives the performance results for various LQR designs and compares them with the SOF design. If the LQR controller is designed without considering the actual gust spectrum, that is, assuming a white noise, then the design is not useful in controlling the response of the assumed gust. This is because, though the LQR is, by design, an optimal controller for any disturbance spatial mode (any distribution of disturbance to the various equations), it assumes that the disturbance is a white-noise process affecting all of the frequencies (and, thus, modes) equally. However, the actual gust spectrum is such that it affects a few lower modes much more than any of the higher modes. Consequently, even if the higher-frequency modes have a lower stability margin, these modes are not as affected due to the lower excitation power and, thus, need not be given control priority over the lower modes. Thus, the results obtained using an LQR (white noise) controller are not good.

Table 6 Comparison of SOF performance with LQR

Sensors configuration	Performance measure	State cost	Control cost
SOF 1h	62.788	53.342	9.446
LQR (white noise)	75.015	75.014	0.00025
LQR (gust model)	48.584	38.968	9.616
LQR (FSF)	62.552	52.938	9.614

Now, if the gust model is included and an LQR controller is designed assuming gust state feedback, it gives the best achievable results. However, this model is inconsistent in that knowledge of the gust state is assumed, whereas by definition it is quite random. Though unachievable, it is a good baseline result for comparison. On the other hand, if a full original model state feedback is designed, the performance gives the best achievable results of constant gain output feedback. It is seen that this result is quite close to that obtained by using only root-curvature and root-curvature-rate feedback. Thus, using just a pair of sensors (root curvature and root-curvature rate), an SOF controller could be designed to give performance within 1% of the performance one would achieve by feeding back all of the 96 states. This again points out that effective SOF controllers could be designed by choosing the right sensors.

In summary, SOF controllers can be effective in gust alleviation with the proper choice of sensor. LQR performance using white-noise disturbance assumptions do not lead to effective controllers. Inclusion of a proper gust model is necessary for optimal performance.

Conclusions

SOF controllers were designed for flutter suppression and gust-load alleviation of a slender wing. SOF controller performance was a strong function of the choice of sensors and the sensor placement. For flutter suppression, root twist and root-twist rate were the most important variables, and, thus, sensing these variables led to an SOF controller with performance equivalent to that of an LQR controller. On the other hand, sensing root curvature was of importance for gust-load alleviation due to the dominant effect of gust on the bending modes.

A nonlinear SOF controller was designed by gain scheduling over various wing displacements (a dominant nonlinearity). The nonlinear SOF controller was implemented along with the complete wing nonlinear aeroelastic simulation and was shown to control LCO generated by large disturbances. An LPF was designed and coupled with the static output feedback to get good rolloff characteristics, leading to robustness with respect to high-frequency dynamics. Also, the gain and phase margins of the SOF controller were calculated and where shown to be close to those of the LQG controller.

Gust-load alleviation characteristics for an SOF controller were again quite close to that of an FSF controller. It was further shown that, although the LQR design is optimal for all disturbances (in terms of the equation affected), it is highly dependent on the gust spectrum (as is SOF). Thus, an LQR design based on a white-noise gust spectrum led to suboptimal results. Knowledge of the gust state is very important for efficient control, so that an LQR controller that is designed assuming knowledge of the gust state gives the best results. However, an LQR design based on feedback of just the system states (an FSF without the gust state) gives performance close to that obtained by SOF with just two sensors.

Acknowledgments

This work was supported by U.S. Air Force Office of Scientific Research Grant F49620-98-1-0032, Technical Monitor, Brian P. Sanders. The authors would like to acknowledge W. Haddad and J. Corrado from the Georgia Institute of Technology for their help in the optimal static output feedback design. They also provided some

parts of the basic static output feedback synthesis code. The authors would also like to acknowledge helpful discussions with A. Calise of the Georgia Institute of Technology.

References

[1]Mukhopadhyay, V., "Flutter Suppression Control Law Design and Testing for the Active Flexible Wing," *Journal of Aircraft*, Vol. 32, No. 1, 1995, pp. 45–51.

[2]Lin, C. Y., Crawley, E. F., and Heeg, J., "Open- and Closed-Loop Results of a Strain-Actuated Active Aeroelastic Wing," *Journal of Aircraft*, Vol. 33, No. 5, 1996, pp. 987–994.

[3]Waszak, M. R., and Srinathkumar, S., "Flutter Suppression for the Active Flexible Wing: A Classical Design," *Journal of Aircraft*, Vol. 32, No. 1, 1995, pp. 61–67.

[4]Mukhopadhyay, V., "Transonic Flutter Suppression Control Law Design and Wind-Tunnel Test Results," *Journal of Guidance, Control, and Dynamics*, Vol. 23, No. 5, 2000, pp. 930–937.

[5]Patil, M. J., Hodges, D. H., and Cesnik, C. E. S., "Nonlinear Aeroelastic Analysis of Complete Aircraft in Subsonic Flow," *Journal of Aircraft*, Vol. 37, No. 5, 2000, pp. 753–760.

[6]Hodges, D. H., "A Mixed Variational Formulation Based on Exact Intrinsic Equations for Dynamics of Moving Beams," *International Journal of Solids and Structures*, Vol. 26, No. 11, 1990, pp. 1253–1273.

[7]Peters, D. A., and Johnson, M. J., "Finite-State Airloads for Deformable Airfoils on Fixed and Rotating Wings," *Symposium on Aeroelasticity and Fluid/Structure Interaction, Proceedings of the Winter Annual Meeting*, AD-Vol. 44, American Society of Mechanical Engineers, Fairfield, NJ, 1994, pp. 1–28.

[8]Patil, M. J., "Nonlinear Aeroelastic Analysis, Flight Dynamics, and Control of a Complete Aircraft," Ph.D. Dissertation, School of Aerospace Engineering, Georgia Inst. of Technology, Atlanta, Georgia, May 1999.

[9]Hodges, D. H., Shang, X., and Cesnik, C. E. S., "Finite Element Solution of Nonlinear Intrinsic Equations for Curved Composite Beams," *Journal of the American Helicopter Society*, Vol. 41, No. 4, 1996, pp. 313–321.

[10]Patil, M. J., Hodges, D. H., and Cesnik, C. E. S., "Limit Cycle Oscillations in High-Aspect-Ratio Wings," *Journal of Fluids and Structures*, Vol. 15, No. 1, 2001, pp. 107–132.

[11]Levine, W. S., and Athans, M., "On the Determination of the Optimal Constant Output Feedback Gains for Linear Multivariable Systems," *IEEE Transactions on Automatic Control*, Vol. AC-15, No. 1, 1970, pp. 44–48.

[12]Syrmos, V. L., Abdallah, C. T., Dorato, P., and Grigoriadis, K., "Static Output Feedback—A Survey," *Automatica*, Vol. 33, No. 2, 1997, pp. 125–137.

[13]Makila, P. M., and Toivonen, H. T., "Computational Methods for Parametric LQ Problems—A Survey," *IEEE Transactions on Automatic Control*, Vol. AC-32, No. 8, 1987, pp. 658–671.

[14]Shanno, D. F., and Phua, K. H., "Numerical Comparison of Several Variable-Metric Algorithms," *Journal of Optimization Theory and Applications*, Vol. 25, 1978, pp. 507–518.

[15]Moerder, D. D., and Calise, A. J., "Convergence of a Numerical Algorithm for Calculating Optimal Output Feedback Gains," *IEEE Transactions on Automatic Control*, Vol. AC-30, No. 9, 1985, pp. 900–903.

[16]Patil, M. J., Hodges, D. H., and Cesnik, C. E. S., "Nonlinear Aeroelasticity and Flight Dynamics of High-Altitude Long-Endurance Aircraft," *Journal of Aircraft*, Vol. 38, No. 1, 2001, pp. 88–94.

[17]Bayon De Noyer, M., and Hanagud, S., "A Comparison of H_2 Optimized Design and Cross-Over Point Design for Acceleration Feedback Control," *Proceedings of the 39th Structures, Structural Dynamics, and Materials Conference*, AIAA, Reston, VA, 1998, pp. 3250–3258.

[18]Bisplinghoff, R. L., Ashley, H., and Halfman, R. L., *Aeroelasticity*, Addison Wesley Longman, Reading, MA, 1955, pp. 685–694.

[19]Belvin, W. K., and Park, K. C., "Structural Tailoring and Feedback Control Synthesis: An Interdisciplinary Approach," *Journal of Guidance, Control, and Dynamics*, Vol. 13, No. 3, 1990, pp. 424–429.